MDPI

Article

Non-Collinear Phase in Rare-Earth Iron Garnet Films near the Compensation Temperature

Dmitry A. Suslov [1,*], **Petr M. Vetoshko** [1,2], **Alexei V. Mashirov** [1], **Sergei V. Taskaev** [3], **Sergei N. Polulyakh** [2], **Vladimir N. Berzhansky** [2] **and Vladimir G. Shavrov** [1]

[1] Kotelnikov Institute of Radioengineering and Electronic, Russian Academy of Sciences, 125009 Moscow, Russia; pvetoshko@mail.ru (P.M.V.); a.v.mashirov@mail.ru (A.V.M.); shavrov@cplire.ru (V.G.S.)

[2] V. I. Vernadsky Crimean Federal University, 295007 Simferopol, Russia; s.polulyakh@gmail.com (S.N.P.); v.n.berzhansky@gmail.com (V.N.B.)

[3] Chelyabinsk State University, 454001 Chelyabinsk, Russia; s.v.taskaev@gmail.com

* Correspondence: sda_53@mail.ru

Abstract: The experimental discovery of the suppression effect of the non-collinear phase in strong magnetic fields near the compensation point in ferrimagnetic structures was made. The observations were carried out using the magneto-optical method by creating a lateral temperature gradient in the plane of the epitaxial films of iron garnets. The non-collinear phase is absent in weak magnetic fields. If an external magnetic field exceeds the first critical value, the non-collinear phase arises near the compensation point. The temperature range of the non-collinear phase expands due to the field increase up to the second critical value. Further field increases conversely reduce the temperature range of the non-collinear phase so that the field above the second critical value causes the disappearance of the non-collinear phase. The effect of the occurrence and suppression of the non-collinear phase is demonstrated on samples of two types of iron garnet films with two and three magnetic sublattices. Phase diagrams of the magnetic states in the vicinity of the critical point are constructed, and it is shown that the region of existence of the non-collinear phase in a two-sublattice magnet is smaller than in a three-sublattice one.

Keywords: magneto-optical method; compensation point; magnetic phases; ferrimagnetic materials

1. Introduction

Currently, ferrimagnetic materials with a compensation temperature are well known [1]. The magnetic compensation temperature T_m is a special point on the temperature dependence of the magnetization of a ferrimagnet at which the magnetizations of oppositely directed magnetic sublattices fully compensate one other and the total spontaneous magnetization of the material becomes zero. The theoretical analysis of the behavior of a multi-sublattice ferrimagnet in an external magnetic field allows the prediction of the existence of three magnetic phases that exist in certain temperature ranges [2]. At low temperatures, the magnetizations of non-equivalent sublattices are antiparallel to each other and collinear with the magnetic field; the resulting magnetization decreases with increasing temperature. At temperatures above T_m, a collinear magnetic structure is realized, with magnetization directions of the sublattices inverted with respect to the low-temperature interval.

In the vicinity of the compensation point, the occurrence of a non-collinear (canted) phase is predicted. In this case, the sublattice magnetizations are non-collinear to each other as well as to the external magnetic field.

Thin films of compensated ferrimagnets based on the combination of rare-earth and transition metals having alloy or multilayer forms are currently considered key materials for spintronics and other modern technology [3]. Thin films of Mn_4N also demonstrate

non-collinear ferrimagnetism and are interesting materials for spintronics applications [4]. Modern investigations of great interest for fundamental physics and applications relate to ultrafast magnetism and optical switching. The prospective materials to explore these phenomena in the non-collinear phase near the magnetization compensation point are thin ferrimagnetic films based on a combination of rare-earth and transition metals [5], such as on cation-substituted iron garnets [6–8].

According to molecular field theory, the temperature range of the existence of the non-collinear magnetic structure expands with increasing magnetic field up to the disappearance of collinear magnetic structures [2,9,10]. However, as far as the authors are aware, this finding has not been experimentally confirmed.

The aim of this work was to experimentally detect and investigate various magnetic phases near the spin-reorientation transition caused by temperature. We studied thin magnetic films of cation-substituted iron garnet using by two types of samples. The samples of the first type had three magnetic sublattices related to iron ions in octahedral garnet positions, iron in tetrahedral positions, and rare-earth gadolinium ions in dodecahedral positions. The second type of samples had two magnetic sublattices represented by octahedral and tetrahedral iron, while all other cations, including rare-earth metals in dodecahedral positions, were non-magnetic ones. To visualize the magnetic phases, we applied the magneto-optical Faraday effect, following the approach proposed in [11]. In order to enhance the Faraday rotation, we selected samples of bismuth-containing garnets. To produce different magnetic phases, we applied the lateral temperature gradient in the film plane. The controlled temperature gradient provides the possibility of observing different magnetic phases in the same sample at the same external magnetic field values.

2. Samples

Two series of 5 μm thick and 10×10 mm bismuth iron garnet films were prepared for experiments using liquid-phase epitaxy [12]. The first type of film, $(BiGd)_3(FeGa)_5O_{12}$, contained magnetic Gd^{3+} (spin I = 5/2) ions in the dodecahedral garnets' positions and magnetic ions Fe^{3+} (spin I = 3/2) in both the tetrahedral and octahedral positions. As a result, there were three magnetic sublattices. The second type film, $(BiYLu)_3(FeGa)_5O_{12}$, had only two magnetic sublattices caused by iron ions.

In both compositions, a small amount of the diamagnetic Ga^{3+} ions substituted the magnetic iron ions. Gallium ions have a preference to occupy tetrahedral positions and dilute the largest iron sublattice. Such diamagnetic dilutions play a primary role in precise tuning the compensation temperature in the second type of samples where the dodecahedral sublattice remained completely non-magnetic. The content of magnetic Gd^{3+} ions in dodecahedral positions was the main contributor to the compensation temperature for the first type of sample. Bismuth, in both compositions, enhances the Faraday rotation, which has achieved record values in ferrites based on it [12–14].

A monocrystalline plate of $(GdCa)_3(GaMgZr)_5O_{12}$ garnet was used as the substrate for the epitaxial synthesis of the bismuth gadolinium iron garnet (first type sample). For the second-type film, a plate of $Gd_3Ga_5O_{12}$ garnet crystal was used as the substrate. Both substrates were plates oriented in the (111) crystal plane.

The magnetic state of the epitaxial films of iron garnet significantly depends on the mismatch between film and substrate lattice parameters. The parameters of the crystal structure of the film, a_F, and of the substrate, a_S, give the mismatch parameter $\Delta a = a_F - a_S$. Large values of the mismatch parameter Δa lead to the appearance of large magnetoelastic stresses and a change in the magnetic anisotropy. We minimized this parameter by choosing the type of substrate and the concentration of ions with the required values of ionic radii. Thus, to synthesize the films of the first type of garnet having elements of a large ionic radius, we used a $(GdCa)_3(GaMgZr)_5O_{12}$ substrate with a large cell parameter a = 1.2495 nm. Gadolinium gallium garnet $Gd_3Ga_5O_{12}$ with a smaller cell parameter, a = 1.2373 nm, was the substrate for the second type of film having the minimum number of big ions.

To measure the mismatch parameter Δa for the studied samples, we applied the X-ray diffraction method, which resulted in $\Delta a_1 = 0.0006$ nm for the first type of sample and $\Delta a_2 = 0.0003$ nm for the second type of sample. To estimate crystalline quality, we utilized X-ray rocking curves, which broaden the diffraction peaks. The half-width of the rocking curves did not exceed 15.0″–15.5″ for the used films. Some synthesis condition details and the XRD crystal quality assessment are provided in the Supplementary Materials (Tables S1 and S2, Figure S1).

The ferromagnetic resonance measurements show that both magnetic films demonstrated magnetic anisotropy of the "easy–axis" type at room temperature so that the direction of the easy axis was perpendicular to the film plane. This result is in good agreement with the shape of the domain structure observed by means of the Faraday effect at room temperature too.

The chemical composition of the magnetic films (Tables 1 and 2) was determined via electron probe microanalysis using a Jeol JSM-6480LV (Tokyo, Japan) scanning electron microscope with an INCA X-Maxn energy-dispersive spectrometer. The analysis was carried out at an accelerating voltage of 10 kV and electric current of 1.4 nA. Standardization of the emission lines was carried out using the standards of $GdPO_4$, $ScPO_4$, Fe, YPO_4, Pt, and $BiTe_2$ for the elements O and Gd, Sc, Fe, Y, Pt, and Bi, respectively. Standard deviations for the elements with concentrations larger than 10% in mass did not exceed 2%. Averaging over six points on each sample was applied.

Table 1. Chemical composition of the sample $(BiGd)_3(FeGa)_5O_{12}$. Metal atoms content recalculated per 12 oxygen atoms (according formula unit).

|	Al	Cr	Fe	Cu	Ga	Gd	Pt	Bi	O
1	0.03	0.02	4.22	0.02	0.56	2.40	0.11	0.62	12.00
2	0.04	0.02	4.20	0.02	0.57	2.40	0.11	0.60	12.00
3	0.04	0.02	4.21	0.02	0.58	2.41	0.11	0.59	12.00
4	0.04	0.02	4.23	0.02	0.59	2.39	0.10	0.58	12.00
5	0.03	0.02	4.22	0.02	0.58	2.40	0.11	0.60	12.00
6	0.05	0.02	4.22	0.01	0.58	2.40	0.11	0.58	12.00

Table 2. Chemical composition of the sample $(BiYLu)_3(FeGa)_5O_{12}$. Metal atoms' content recalculated per 12 oxygen atoms (per formula unit).

	Ca	Fe	Ga	Y	Gd	Lu	Pt	Bi	O
1	0.02	3.52	1.45	0.88	0.01	1.30	0.04	0.78	12.00
2	0.02	3.51	1.45	0.87	0.02	1.32	0.02	0.78	12.00
3	0.02	3.51	1.47	0.84	0.01	1.32	0.03	0.78	12.00
4	0.03	3.50	1.45	0.86	0.01	1.32	0.03	0.79	12.00
5	0.03	3.49	1.47	0.87	0.02	1.31	0.03	0.78	12.00
6	0.03	3.51	1.45	0.86	0.02	1.31	0.03	0.79	12.00

As a first approach, we assumed that the chemical composition of the studied iron garnets contained 12 oxygen ions per formula unit. Using this assumption, we obtained the cation content per formula unit too (Tables 1 and 2). By combining these data together with known molecular field coefficients [15], we estimated the temperature of magnetic compensation and found a good agreement between molecular field theory and the experimental results.

To define the temperature of magnetic compensation, we used the temperature dependence of magnetization measured using vibrating magnetometry. Figure 1 gives the dependences obtained by using a Versa Lab setup (Quantum Design, Sao Paolo, Brazil) for both samples in a weak magnetic field of 10 mT applied perpendicular to the film plane. Both dependencies (Figure 1) had a qualitatively similar characteristic, which is typical for a ferrimagnetic material with a magnetic compensation temperature. The temperature of

magnetic compensation is a temperature that results the deep minimum of the magnetization dependence below the Neel temperature. The absolute magnetization value is an unimportant feature in finding the temperature of magnetic compensation. This allowed us to ignore the normalization of the measured magnetic moment on the film volume and to present magnetization in the arbitrary units.
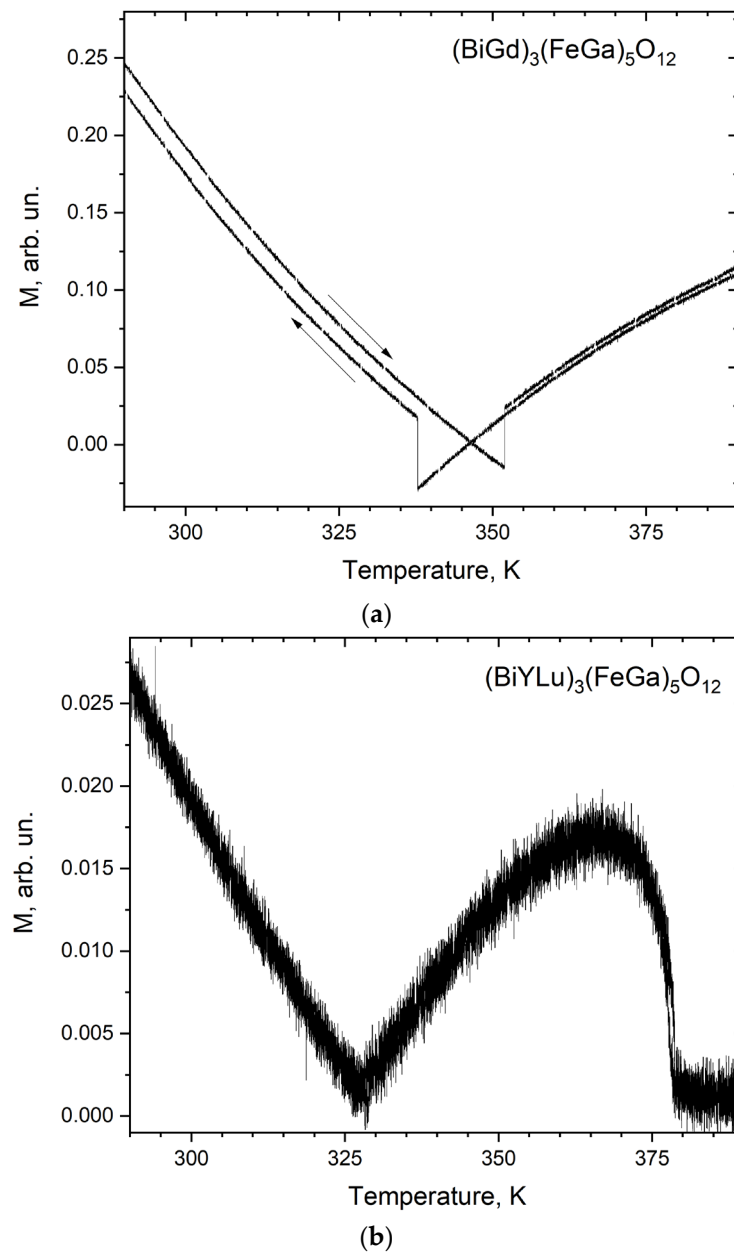

Figure 1. Temperature dependences of magnetization. External magnetic field of 0.01 T directed along film normal. The speed of temperature scanning was about 1 K/min. (**a**) $(BiGd)_3(FeGa)_5O_{12}$, (**b**) $(BiYLu)_3(FeGa)_5O_{12}$.

The special measurements of the substrate magnetization indicate the absence of any features that can affect the accuracy of finding the compensation temperature. The substrate paramagnetic magnetization decreases $1/T$ as the temperature T grows, and paramagnetic contribution is excluded from the samples' magnetization in Figure 1. As a result, we found a compensation temperature $T_m = 346.5$ K for the first type of sample (bismuth gadolinium iron garnet having three magnetic sublattices) and $T_m = 327.5$ K for the second type of sample (bismuth iron garnet having two magnetic sublattices).

3. Experiment

The experimental method used in this study is based on the gradient in-plane method proposed in [16,17] for observing phase transitions. In contrast to [16,17], we used a temperature gradient instead of the gradient of the composition in the film plane. The general scheme of the experiment is shown in Figure 2.
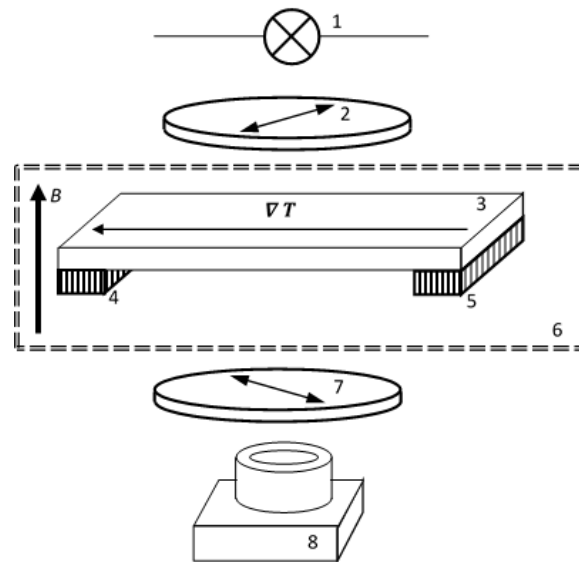
Figure 2. General scheme of the experiment. 1—unpolarized light source, 2—polarizer, 3—film sample, 4—heating Peltier element, 5—cooling Peltier element, 6—temperature-controlled stage, 7—analyzer, and 8—camera and microscope at 550× magnification, *B*—magnetic field, ∇T—lateral temperature gradient.

Polarized light was used to observe the magnetic phases. Passing through the magnetic film of the sample, the polarized light entered the digital camera through the analyzer. The angle between the polarizer and the analyzer was adjusted to achieve the maximum image. This provided some middle intensity of light if polarization remained unchanged between the polarizer and analyzer.

Due to the Faraday effect, polarization rotation is possible in magnetic materials that influence the intensity of the light passing through a film. The Faraday rotation in our samples provided the dominant contribution from the magnetic sublattice of the tetrahedral iron ions. The diamagnetic bismuth ions only enhanced this effect. The contribution of the octahedral sublattice was always less than that of the tetrahedral one. The angle of Faraday rotation depends on the projection of the tetrahedral magnetization onto the direction of the light beam and reaches the maximum value when magnetization is collinear to the beam, while the orthogonal direction results in unchanged polarization. As a result, the sample areas having different tetrahedral magnetization along the film normal should demonstrate different brightness in the image obtained with the digital camera.

In the experiments, a digital video camera was used together with a 550× magnification microscope. The observed area of the sample was a circle with a diameter of about 3 mm. A special holder made of non-magnetic materials was made for both the video camera and the microscope.

To create a lateral temperature gradient ∇T in the sample plane, two Peltier elements connected in opposite directions were used. Both Peltier elements, model TB–7–06–08 KryoTherm (St. Petersburg, Rusia) with a size of 4 × 4 mm, were located at the edges of the observation area at a distance of 3 mm. A temperature-controlled sample holder with Peltier elements was used to stabilize the temperature during measurements. The sample temperature monitoring and control system also included service elements, such as a temperature sensor and a differential thermocouple for monitoring the temperature

gradient, not shown in Figure 2. The specially designed holder that held the optical system together, described above, temperature control equipment, and the test sample were placed in the working area of a superconducting magnet. The magnet provided a field *B* up to 10 T directed along the normal to the film plane. The cryogenic system for the superconducting magnet was a GFSG-510-2K-SCM10T-VTI29 (CryoTrade Engineering LLC, Moscow, Russia).

To automate the experiment, a computer, a temperature control system, measuring instruments, and a magnet power supply were networked. A computer managed the network utilizing the specially developed software. The developed system automatically stored into a file the measured values of magnetic field, temperature, and temperature gradient and displayed them on a monitor.

The magnetization redistribution due to the changing magnetic field resulted in the changing image registered with polarized light. The dynamically changing image together with the above-mentioned parameters were recorded as a video file. The proposed optical system along with the temperature and magnetic field management systems allowed the visualization of the magnetization behavior during the temperature-phase transition in high-quality, homogeneous films.

4. Results and Discussion

To identify the conditions for the existence of a non-collinear phase, measurements were carried out in magnetic fields ranging from 0 to 10 T. The sample temperature was maintained in the compensation temperature region.

Visually, both types of samples qualitatively demonstrated the same behavior, differing only in numerical values. The images for the $(BiYLu)_3(FeGa)_5O_{12}$ sample looked more contrasted than those for the first type sample, because the concentration of Bi ions in the second type of sample was significantly higher (Tables 1 and 2). The experimental results for the second type of sample are given in Figures 3 and 4.

In the absence of an external magnetic field, a large-block domain structure was observed at room temperature, and the temperature variations changed this structure. In magnetic fields exceeding the coercivity threshold, the sample was in saturation, and a monodomain state was observed.

To conduct experiments near the compensation point, we started from room temperature and gradually heated the sample up to the compensation point. The rate of temperature changes did not exceed 1 degree per minute.

Near the compensation temperature, the observed pattern consists of two areas of different brightness when the magnetic field is below the first critical value H_{c1} (Figure 3a). We attribute these areas to collinear phases of different magnetization directions perpendicular to the film plane. The observed behavior agreed with expectations because the theoretical temperature range for the canted phase existence is sufficient in low fields [2,10]. The other argument is that the "easy-axis" magnetic anisotropy crushes the canted phase in low fields. This anisotropy also responds to the temperature hysteresis in the magnetization near the compensation point (Figure 1a). Similar hysteresis took place for the second type of sample in the 1 mT field.

Let us note that the visualized magnetic phases differed from one other in the direction of the magnetization of tetrahedral iron, while the direction of the total magnetization was the same for both phases and laid along the magnetic field. A boundary between areas of the different phases is the 180-degree compensation wall. This compensation wall is similar to the compensation wall that has been reported in [17,18]. Unlike the temperature gradient reported here, the authors of [17,18] used samples that had a compensation point gradient due to the gradient of the chemical composition in a sample.

Starting from the first critical value H_{c1}, the field increase brought the extra features into the observed pattern. A transition region of intermediate brightness appears between regions that represent collinear phases (Figure 3b). The field growth up to the second critical value H_{c2} increased the width of the transition region.
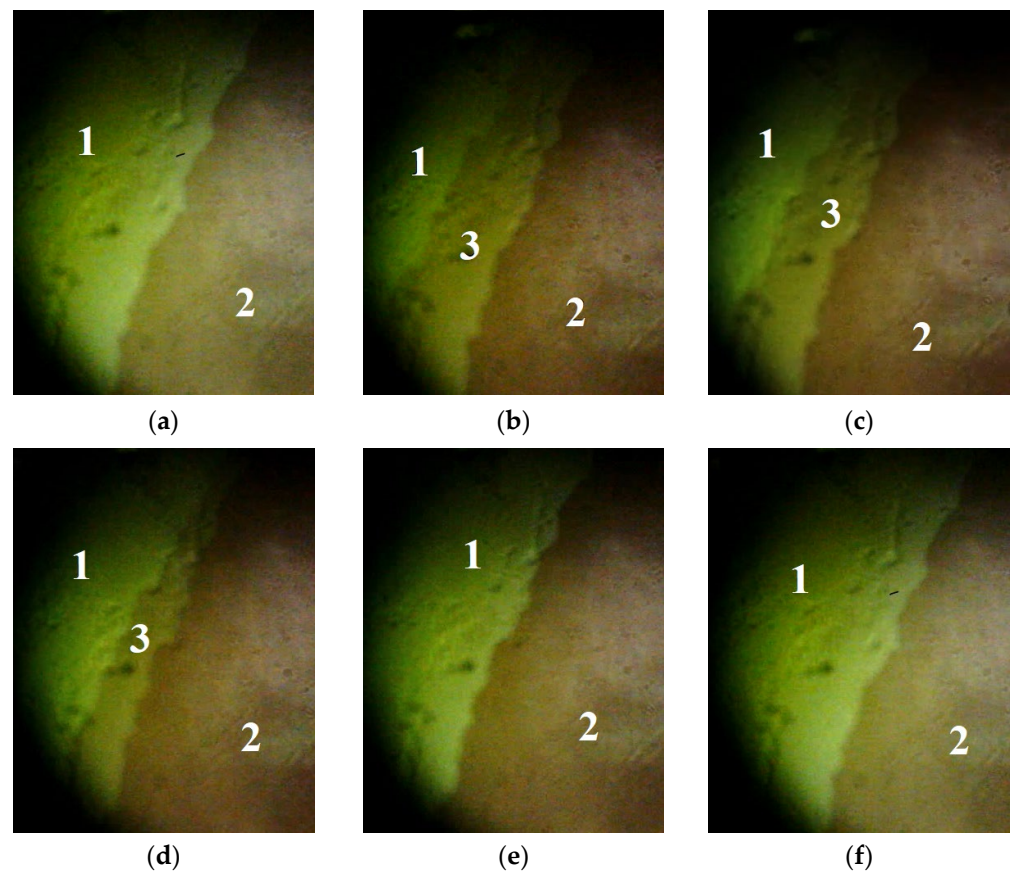
Figure 3. Magneto-optical visualization of phase states in the $(BiYLu)_3(FeGa)_5O_{12}$ sample at the temperature T = 327.5 K (the region of magnetic compensation) in an external magnetic field B = 0.5 T (**a**), B = 1.0 T (**b**), B = 1.03 T (**c**), B = 1.05 T (**d**), B = 1.1 T (**e**), and B = 1.2 T (**f**). (1), (2) Collinear phases of opposite magnetization direction; (3) non-collinear (canted) magnetic phase.
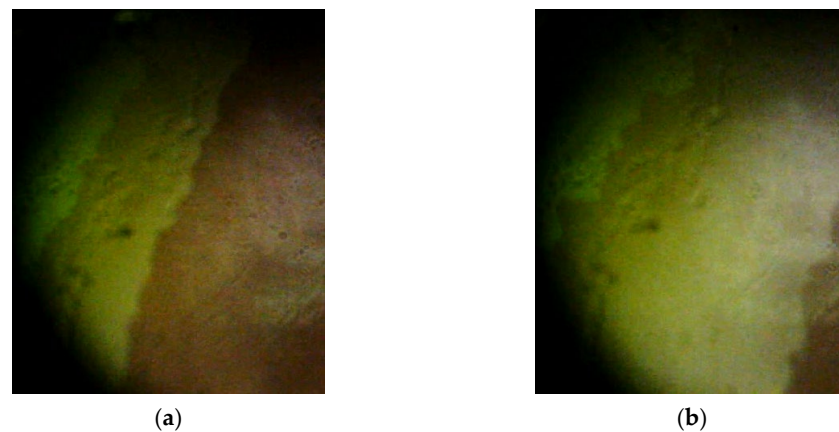
Figure 4. The temperature gradient influence on the non-collinear phase in the $(BiYLu)_3(FeGa)_5O_{12}$ sample. The lateral gradient for image (**a**) is approximately twice as small as that in image (**b**).

The new region appeared due to the canted phase, which gave a weaker Faraday rotation. In reality, the directions of the sublattices magnetization do not match the external magnetic field in the non-collinear (canted) phase. At the temperature of magnetic compensation, the sublattices' magnetizations are practically orthogonal to the external field and, as a result, provide a vanishingly small contribution to the Faraday rotation. The temperature offset from the compensation point results in out-of-plane magnetization. The angle between the magnetization and a perpendicular to the film plane should change smoothly in the canted phase [2].

This theoretical expectation contradicts the experimental results, which showed a sharp boundary between the canted and collinear phases. However, the sharp boundary occurred in the region of fields and temperatures where the coexistence of both collinear and canted phases was possible. A similar pattern was observed by magneto-optical method in experimental work [17].

With an increase in the magnetic field strength, the area corresponding to the non-collinear phase initially increased, and then, starting from the second critical field H_{c2}, it decreased. It can be seen that the canted phase region in the external field of 1.03 T (Figure 3c) was smaller than in the field of 1.0 T (Figure 3b). At external magnetic field strengths above a certain critical value, H_{c3}, the non-collinear phase completely disappeared, and two opposite collinear phases with maximum contrast were observed again (Figure 3e). A further increase in the intensity of the external magnetic field did not change anything in the observed picture (Figure 3f).

This experimental result conflicts with known theories [2,10]. According to theory, an increase in a magnetic field should only increase the width of the temperature region where a canted phase exists. The other problem relates to the maximum width of the temperature range for the canted phase. This region is too small, contrary to expectations.

On the other hand, we obtained preliminary results in the scope of molecular field theory. We found an extra magnetization in the collinear phase due to the paraprocess. This can narrow the temperature region of the canted phase and contribute to a decrease in the collinear phase energy in strong magnetic fields. As mentioned above, for a fixed magnetic field, the magnetization direction depends on the temperature in the canted phase. The temperature gradient induces an inhomogeneity in the magnetization direction for the canted phase. As a result, this can contribute to an increase in canted phase energy. These results will be discussed in detail in the next publication.

For the temperature gradient used for the magneto-optical visualization, we could tune it in the range from 0 K per cm to 12 K per cm. The most effective influence on the magnetic phase images was exerted by a temperature gradient in the range from 1.5 K per cm to 2.5 K per cm. Further gradient increases had little effect on the visualization quality but had a general temperature effect on the sample, moving the phase boundary out of the observation area. The data in Figure 4 demonstrate the influence of the lateral temperature gradient. The lateral gradient for the image in Figure 4b is approximately twice as large as that for the image in Figure 4a, while the sample temperature and external magnetic field are approximately the same for both cases.

The experiments showed that the value of the third critical field H_{C3} = 3.2 T for a three-sublattice bismuth gadolinium iron garnet having Neel temperature T_N = 450 K was almost three times higher than that for a two-sublattice $(BiYLu)_3(FeGa)_5O_{12}$ garnet that had a Neel temperature T_N = 380 K and H_{C3} = 1.1 T.

Determined experimentally, phase diagrams in the coordinate system of magnetic field vs. temperature for samples of both types are given in Figure 5 and Table 3. The arrows (Figure 5) schematically represent the sublattices' magnetizations.

Below the compensation temperature in the second type of sample (Figure 5b) dominated the octahedral magnetization, and it was directed along the magnetic field in the collinear phase. Above the compensation temperature, vice versa, it was dominated by the tetrahedral sublattice. In the canted phase, the deviation from the antiparallel magnetization arrangement was small, in the order of several degrees (our estimations using molecular field theory). A change in temperature primarily changed the angle between the magnetizations and the field, so that the magnetizations remained almost antiparallel to one other. Although the bismuth gadolinium garnet had three magnetic sublattices, the net iron magnetization could be considered as a single one. As a result, we could consider the first type of sample as a ferrimagnet of two magnetic sublattices, where one sublattice was gadolinium, and the other sublattice was iron (Figure 5a).

(a)

(b)
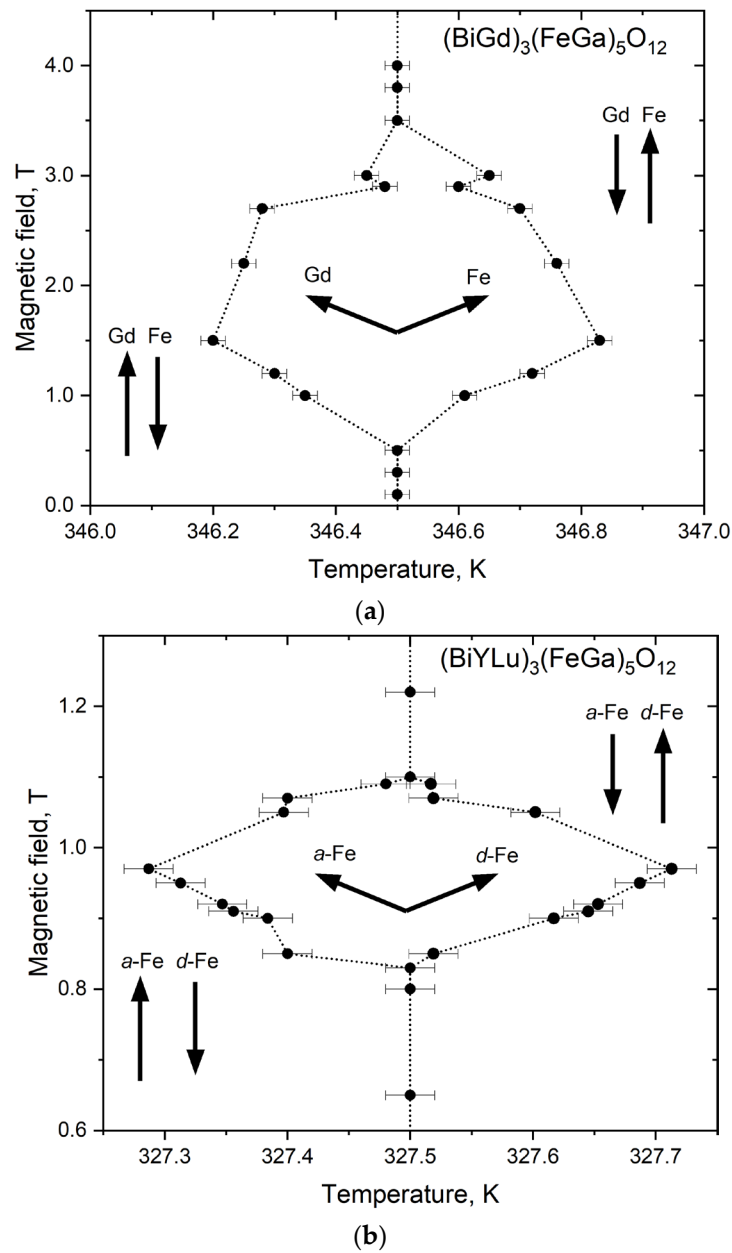
Figure 5. Phase diagrams in the vicinity of the compensation point in samples: (**a**) $(BiGd)_3(FeGa)_5O_{12}$; (**b**) $(BiYLu)_3(FeGa)_5O_{12}$. Arrows schematically represent sublattices magnetizations for Gd, total (Fe), octahedral (a-Fe), and tetrahedral (d-Fe) iron.

Table 3. Main characteristics of samples and their phase diagrams.

N	Composition	T_m, K	T_N, K	H_{c1}, T	H_{c2}, T	H_{c3}, T	dH, T	dT, K
1	$(BiGd)_3(FeGa)_5O_{12}$	346.5	450	0.5	1.5	3.2	2.7	0.6
2	$(BiYLu)_3(FeGa)_5O_{12}$	327.5	380	0.65	0.95	1.1	0.45	0.4

It can be seen that the magnetic field interval $dH = H_{C3} - H_{C1}$ and temperature interval $dT = T_{max} - T_{min}$, that define the area of a non-collinear phase near the compensation point had different values for the studied samples. The field interval $dH_1 = 3$ T and temperature range $dT_1 = 1$ K for the three-sublattice garnets were visibly larger than $dH_2 = 0.5$ T, $dT_2 = 0.7$ K for the two-sublattice garnet. The difference in behavior between the two types of structures is related to the difference in exchange interactions between them, as well

as to the possible influence of magnetic anisotropy, the role of which in the formation of phase diagrams for iron garnet films near the compensation point requires more detailed theoretical consideration.

5. Conclusions

We experimentally demonstrated that the lateral temperature gradient permits the observation of three different magnetic phases (two collinear and one canted) in the same sample in the same magnetic field. The result was achieved for the cation-substituted iron garnet by means of the Faraday effect.

Phase T–H diagrams of the magnetic states in two- and three-sublattice ferrimagnetic structures in the vicinity of the compensation point were experimentally determined using magneto-optical methods. Below the critical field H_{c1}, two collinear magnetic phases separated by a compensational domain boundary were observed. In addition to collinear magnetic phases, a region of non-collinear magnetic phase was experimentally observed above this value. Starting from a certain field H_{c2}, the temperature range of the existence of the non-collinear phase decreased and, at H_{c3}, a phase transition to the collinear phase occurred.

Further theoretical and experimental studies should clarify the features of the magnetic phase T–H diagrams of rare-earth iron garnets near the spin-reorientation phase transition point.

References

1. Belov, K.P. Ferrimagnets with 'weak' magnetic sublattice. *Physics–Uspekhi* **1996**, *6*, 623–634. [CrossRef]
2. Clark, A.E.; Callen, E. Néel Ferrimagnets in Large Magnetic Fields. *J. Appl. Phys.* **1968**, *39*, 5972–5982. [CrossRef]
3. González, J.A.; Andrés, J.P.; Antón, R.L. Applied Trends in Magnetic Rare Earth/Transition Metal Alloys and Multilayers. *Sensors* **2021**, *21*, 5615. [CrossRef] [PubMed]
4. He, Y.; Lenne, S.; Gercsi, Z.; Atcheson, G.; O'Brien, J.; Fruchart, D.; Rode, K.; Coey, J.M.D. Noncollinear ferrimagnetism and anomalous Hall effects in Mn4N thin films. *Phys. Rev. B* **2022**, *106*, L060409. [CrossRef]
5. Xu, C.; Weng, J.; Li, H.; Xiong, W. The study of ultrafast magnetization reversal across magnetization compensation temperature in GdFeCo film induced by femtosecond laser pulses. *J. Magn. Magn. Mater.* **2014**, *352*, 25–29. [CrossRef]
6. Deb, M.; Molho, P.; Barbara, B.; Bigot, J.-Y. Controlling laser-induced magnetization reversal dynamics in a rare-earth iron garnet across the magnetization compensation point. *Phys. Rev. B* **2018**, *97*, 134419. [CrossRef]
7. Mashkovich, E.A.; Grishunin, K.A.; Zvezdin, A.K.; Blank, T.G.H.; Zavyalov, A.G.; van Loosdrecht, P.H.M.; Kalashnikova, A.M.; Kimel, A.V. Terahertz-driven magnetization dynamics of bismuth-substituted yttrium iron-gallium garnet thin film near a compensation point. *Phys. Rev. B* **2022**, *106*, 184425. [CrossRef]
8. Logunov, M.; Safonov, S.; Fedorov, A.; Danilova, A.; Moiseev, N.; Safin, A.; Nikitov, S.; Kirilyuk, A. Domain Wall Motion Across Magnetic and Spin Compensation Points in Magnetic Garnets. *Phys. Rev. Appl.* **2021**, *15*, 064024. [CrossRef]
9. Zvezdin, A.K.; Matveev, V.M. Some Features of the Physical Properties of Rare-Earth Iron Garnets Near the Compensation Temperature. *Sov. Phys. JETP* **1971**, *35*, 140–145.
10. Bernasconi, J.; Kuse, D. Canted Spin Phase in Gadolinium Iron Garnet. *Phys. Rev. B* **1971**, *3*, 811–815. [CrossRef]

11. Vetoshko, P.M.; Berzhansky, V.N.; Poluliach, S.N.; Suslov, D.A.; Mashirov, A.V.; Shavrov, V.G.; Pavliuk, E.V. Magneto-optical visualization of magnetic phases in an epitaxial garnet ferrite film near the compensation point. In Proceedings of the ICEEE-2022, RF, Alushta, Ukraine, 27 September–1 October 2022.

12. Prokopov, A.R.; Vetoshko, P.M.; Shumilov, A.G.; Shaposhnikov, A.N.; Kuz, A.N.; Koshlyakova, N.N.; Berzhansky, V.N.; Zvezdin, A.K.; Belotelov, V.I. Epitaxial Bi-Gd-Sc iron-garnet films for magnetophotonic applications. *J. Alloys Compd.* **2016**, *671*, 403–407. [CrossRef]

13. Zvezdin, A.K.; Kotov, V.A. *Modern Magnetooptics and Magnetooptical Materials*; CRC Press: Boca Raton, FL, USA, 1997; Volume 404, ISBN 9780367579494.

14. Shaposhnikov, A.N.; Berzhansky, V.N.; Prokopov, A.R.; Milyukova, E.T.; Karavaynikov, A.V. Interface properties single crystal films bismuth-constituted garnet—GGG substrate. *Scientific Notes of Taurida V. I. Vernadsky Univ. Ser. Phys.* **2009**, *22*, 127–141.

15. Hansen, P.; Röschmann, P.; Tolksdorf, W. Saturation magnetization of gallium-substituted yttrium iron garnet. *J. Appl. Phys.* **1974**, *45*, 2728–2732. [CrossRef]

16. Lisovskii, F.V.; Shapovalov, V.I. Noncollinearity of sublattices and existence of a domain structure in $Dy_3Fe_5O_{12}$ near the magnetic-compensation point in strong magnetization fields. *JETP Lett.* **1974**, *20*, 128–131.

17. Lisovskii, F.V.; Mansvetova, E.G.; Shapovalov, V.I. Phase diagram and domain-boundary structure in a uniaxial ferrimagnet near the compensation point. *Sov. Phys. JETP* **1976**, *44*, 755–760.

18. Hansen, P.; Krumme, J.-P. The compensation wall. *Philips Tech. Rev.* **1974**, *34*, 96–102.

19. Blank, S.L.; Nielsen, J.W. The growth of magnetic garnets by liquid phase epitaxy. *J. Cryst. Growth* **1972**, *17*, 302–311. [CrossRef]